

Flux-driven Josephson parametric amplifier

T. Yamamoto,^{1,2,3} K. Inomata,² M. Watanabe,² K. Matsuba,^{3,4} T. Miyazaki,³ W. D. Oliver,⁵ Y. Nakamura,^{1,2,3} and J. S. Tsai^{1,2,3}

¹*NEC Nano Electronics Research Laboratories, Tsukuba, Ibaraki 305-8501, Japan*

²*Emergent Materials Department, The Institute of Physical and Chemical Research (RIKEN), Wako-shi, Saitama 351-0198, Japan*

³*CREST-JST, Kawaguchi, Saitama 332-0012, Japan*

⁴*Department of Materials Sciences and Engineering, Tokyo Institute of Technology, 4259 Nagatsuta-cho, Midori-ku, Yokohama, 226-8503, Japan*

⁵*MIT Lincoln Laboratory, 244 Wood Street, Lexington, Massachusetts 02420, USA*

(Dated: February 2, 2022)

We have developed a Josephson parametric amplifier, comprising a superconducting coplanar waveguide resonator terminated by a dc SQUID (superconducting quantum interference device). An external field (the pump, ~ 20 GHz) modulates the flux threading the dc SQUID, and, thereby, the resonant frequency of the cavity field (the signal, ~ 10 GHz), which leads to parametric signal amplification. We operated the amplifier at different band centers, and observed amplification (17 dB at maximum) and deamplification depending on the relative phase between the pump and the signal. The noise temperature is estimated to be less than 0.87 K.

Degenerate parametric amplifiers are phase sensitive amplifiers, which can in principle amplify one of the two quadratures of a signal without introducing extra noise.^{1,2} Parametric amplifiers based on the nonlinear inductance of a Josephson junction have been studied for a long time,³ including one which demonstrated vacuum noise squeezing.⁴ Recently, there has been a renewed interest in parametric amplifiers^{5,6,7} due in part to the increasing need for quantum-limited amplification in the field of quantum information processing using superconducting circuits.^{8,9}

In the present work, we design a Josephson parametric amplifier, comprising a superconducting transmission-line resonator terminated by a dc SQUID (superconducting quantum interference device). Contrary to the previous works, the pump is not used to directly modulate a current through the Josephson junction, but is instead used to modulate a flux through the dc SQUID.¹⁰ The resonant frequency of the resonator, namely, the band center of the signal, is widely controllable by a dc flux also applied to the SQUID (see also Ref. [7]). Moreover, as the pump and the signal are applied to different ports and their frequencies are twice different (see below), it is straightforward to separate the output signal from the pump. This is a unique property of the flux-pumping scheme; it arises because the finite dc flux bias allows linear coupling of the pump even in the absence of a dc current bias across the SQUID.¹¹ We operated such a flux-driven parametric amplifier and characterized its basic properties.

Figure 1a shows a schematic diagram of the flux-driven parametric amplifier. The primary component of the amplifier is a transmission-line resonator defined by its coupling capacitance C_c and a dc SQUID termination. The magnetic flux Φ penetrating the SQUID loop changes the boundary condition of the resonator at the right end (by the change of the Josephson inductance), and hence enables us to control the resonant frequency.^{12,13} The res-

onant frequency f_0 for the first mode ($\lambda/4 \geq d$, where λ is the wavelength and d is the cavity length) is schematically drawn as a function of Φ/Φ_0 in Fig. 1b, where Φ_0 is a flux quantum (see also Fig. 2a). We now assume the cavity resonance is set to a particular value, f_{0dc} , by applying a dc flux Φ_{dc} (open circle in the figure). We then apply microwaves at a frequency $2f_{0dc}$ to the pump line which is inductively coupled to the SQUID loop. The pump microwaves modulate Φ and, hence, f_0 about its static value f_{0dc} at $2f_{0dc}$. This modulation does parametric work for the signal microwaves at f_{0dc} which comes into the resonator. The amplified (or deamplified) signal is then reflected back along the signal line. Note that the leakage of the pump microwaves into the signal port is suppressed, because the second resonance mode does not exist around $2f_{0dc}$.

The device was fabricated using the planarized niobium trilayer process at MIT Lincoln Laboratory. The coplanar-waveguide resonator is made by patterning a 150-nm-thick niobium film deposited on an oxidized silicon substrate. It consists of a center conductor (10 μm wide and 2.6 mm long) and two lateral ground planes nearby. The coupling capacitance C_c was designed to be 16 fF. The critical current of the Josephson junctions for the SQUID was estimated to be 1.5 μA per each from the process test data. The self-inductance of the SQUID loop and the mutual inductance between the SQUID loop and the pump line were estimated by a numerical calculation to be 34 and 5 pH, respectively. The field for the dc flux bias was generated by a superconducting solenoid, which is attached below the sample package.

All measurements were done using a dilution refrigerator at the base temperature of 30 mK. Figure 1c is a schematic diagram of the measurement setup. We used a directional coupler, which gave 20-dB attenuation to the input signal, to measure the reflected microwaves from the resonator. We also used a cryogenic high electron mobility transistor (HEMT) amplifier with a gain of 38

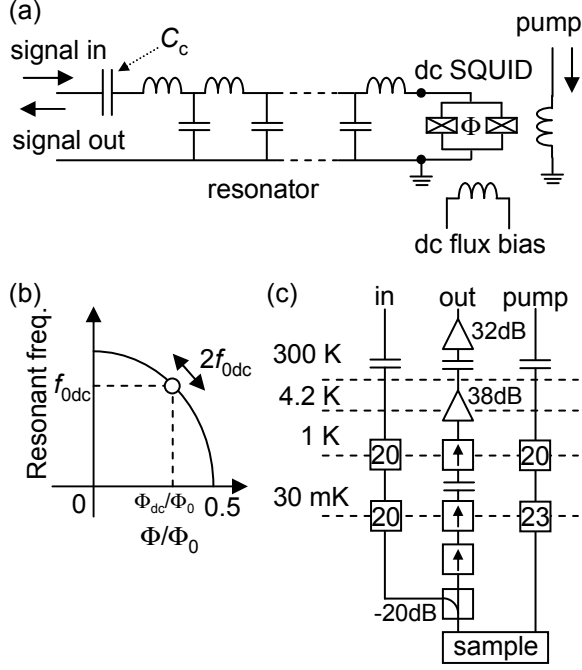


FIG. 1: (a) Schematic circuit diagram of the flux-driven Josephson parametric amplifier. (b) Operation principle of the parametric amplifier. Solid curve represents the resonant frequency of the cavity. Ac flux modulation induces the modulation of the resonant frequency about its static value f_{0dc} , which leads to the parametric amplification. (c) Schematic diagram of the measurement setup. Squares with a number inside represent fixed attenuators with corresponding attenuation in dB. Squares with an arrow inside represent isolators.

dB and a noise temperature T_N^{HEMT} of 9 K at 10 GHz. The frequency band for the signal line, which is limited by the isolators, is roughly from 9 to 11 GHz.

First, we characterized the resonator using a vector network analyzer connected to the “in” and “out” ports in Fig. 1c. All power levels shown below refer to the input or the output of the sample box, where gains or losses of the components (e.g. HEMT amplifiers and attenuators) in the measurement lines have been calibrated away within an accuracy of ± 2 dB. Under a fixed dc flux bias, we observe a 2π rotation of the phase of the reflection coefficient Γ , which is measured as the scattering parameter S_{21} , at the resonant frequency. The inset of Fig. 2a shows an example for $\Phi/\Phi_0 = 0.34$, from which the quality factor of the resonator is estimated to be 250.¹⁴ Here the power of the input signal P_s is sufficiently low (-136 dBm).

The resonant frequency f_{0dc} exhibits a periodic dependence on Φ/Φ_0 . It becomes maximal (11.16 GHz) at $\Phi/\Phi_0 = m$ and decreases as we approach $\Phi/\Phi_0 = m + 1/2$, where m is an integer (see Fig. 1b). A part of the modulation is shown in Fig. 2a. The minimum is not exactly at 0.5 because of the nonzero loop inductance of the dc SQUID.

Next, we performed similar measurements in the pres-

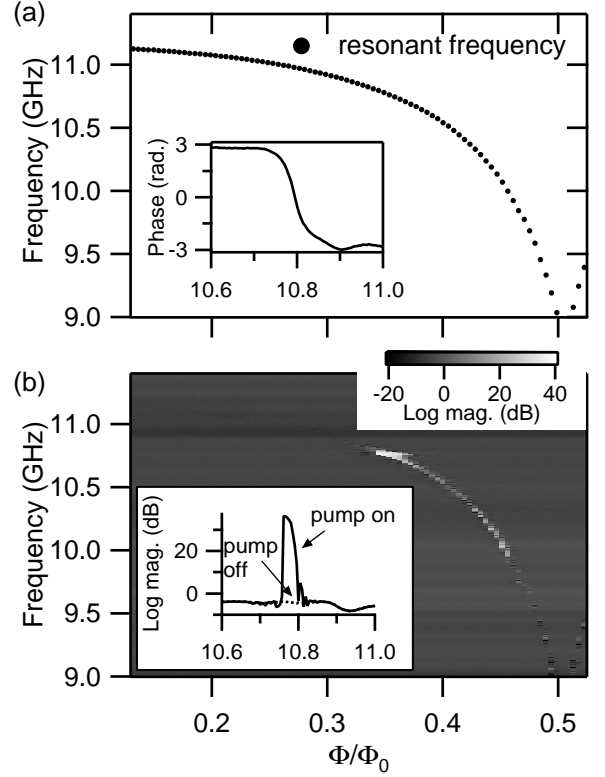


FIG. 2: (a) Resonant frequency as a function of the normalized magnetic flux. The inset shows the phase of the reflection coefficient Γ as a function of the frequency in GHz at $\Phi/\Phi_0 = 0.34$. (b) An intensity plot of $|\Gamma|$ (pump on) as a function of the signal frequency and the normalized magnetic flux. The inset shows a cross section at $\Phi/\Phi_0 = 0.34$ together with the data when the pump is off.

ence of the pump microwaves applied to the “pump” port. Figure 2b is an intensity plot of the Γ amplitude as a function of the signal frequency f_s and Φ/Φ_0 . As f_s is swept by the network analyzer, the pump frequency f_p , which is generated by another microwave source, is synchronously swept such that $f_p = 2f_s$. The power of the pump microwaves P_p is -66 dBm. We observe amplified signals near the corresponding resonant frequencies. The bright spot near $\Phi/\Phi_0 = 0.34$ is observed even without input signal when P_p is larger than -72 dBm. As shown in the inset, which is a cross section at $\Phi/\Phi_0 = 0.34$, the gain looks much larger than those shown later. Here, the device is working as an oscillator rather than an amplifier.

To further characterize the amplifier, we studied the phase dependence of the gain, a hallmark of degenerate parametric amplifiers, using two phase-locked microwave generators. The signal at f_s was amplitude modulated at 10 kHz and applied to the signal input. The pump at $f_p = 2f_s$ (twice the carrier of the input signal) was applied to the pump port. A spectrum analyzer was used to detect the output power at the side-band frequency ($f_s + 10$ kHz). Figure 3a shows the side-band peak mea-

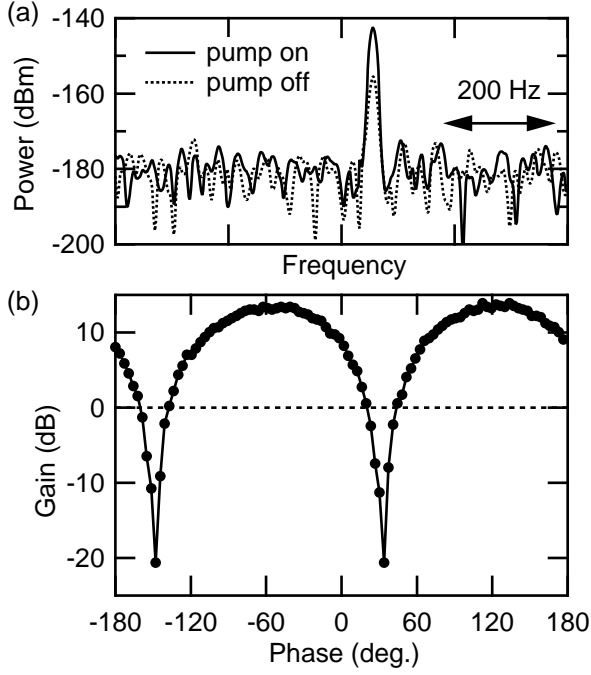


FIG. 3: (a) Side-band peak measured by the spectrum analyzer. The peak is located at 10.78 GHz + 10 kHz (carrier + modulation). The solid curve is a spectrum when the pump is on, while the dashed curve is a spectrum when the pump is off. (b) Gain as a function of the carrier phase of the signal.

sured by the spectrum analyzer with 10-Hz resolution bandwidth and video bandwidth. For comparison, the trace when the pump is turned off is also plotted. Here, $f_{0dc} = 10.77$ GHz, $f_s = 10.78$ GHz, $f_p = 21.56$ GHz, $P_s = -148$ dBm, and $P_p = -71$ dBm. We intentionally detuned f_s from f_{0dc} to avoid having emission without an input field, as was mentioned earlier. We defined the gain as the difference between the two side-band peak values and studied how it depends on the relative phase between the carriers of the signal and the pump.

Figure 3b shows the gain as a function of the carrier phase of the signal. As expected, it shows a periodic dependence with a period of π . The maximum gain is 14 dB.¹⁵ At certain phases, the peak value becomes lower than the pump-off level, and the gain is negative. This is the so-called deamplification, a key property associated with noise squeezing.^{4,16}

Figure 4 shows the maximum value of the phase-dependent gain as a function of P_s . In the case of $f_s = 10.78$ GHz, the maximum gain decreases quickly at $P_s > -130$ dBm. The lower bound is not determined by the parametric amplifier itself, but by the noise of the measurement setup, which is dominated by the noise of the HEMT amplifier. The gain suppression at high P_s is closely related to the nonlinear inductance of the Josephson junctions. Without pumping, we observe a hysteretic behavior (bifurcation) in the frequency dependence of Γ at above $P_s = -101$ dBm. Also, at high P_s , we observe a

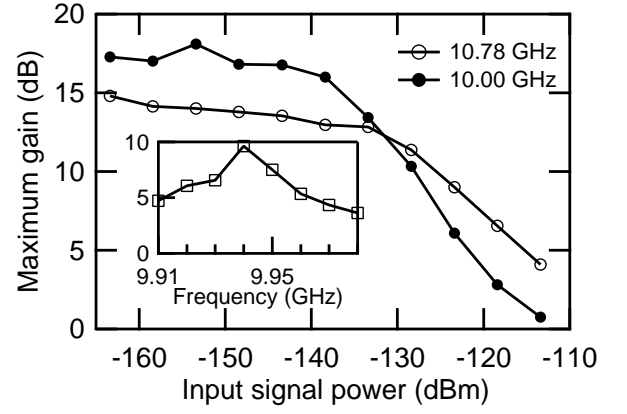


FIG. 4: Maximum gain as a function of the input signal power P_s . For $f_s = 10.00$ GHz and 10.78 GHz, $f_{0dc} = 10.00$ GHz and 10.77 GHz, respectively. The inset shows a maximum gain as a function of the input signal frequency for $f_{0dc} = 9.94$ GHz.

distorted (sawtooth-like) curve in the phase dependence of the gain, which becomes conspicuous above $P_s \sim -120$ dBm (data not shown).

As we mentioned, one of the advantages of the present parametric amplifier is the controllability of the band center. To demonstrate this, we adjusted Φ_{dc} so that $f_{0dc} = 10.00$ GHz and operated the amplifier at $f_s = 10.00$ GHz, $f_p = 20.00$ GHz, and $P_p = -71$ dBm. Qualitatively the same phase dependence was observed, and the maximum gain as a function of P_s is plotted in Fig. 4. Although the dynamic range is narrower because of a smaller critical current of the dc SQUID, a gain of 17 dB is attained.

A bandwidth at fixed f_{0dc} was also investigated, as exemplified in the inset of Fig. 4. Here, f_{0dc} is set to be 9.94 GHz, and f_s was varied around f_{0dc} . For each f_s , we performed a phase-dependence measurement to determine the maximum gain, and plot it as a function of f_s . We set $f_p = 2f_s$, $P_s = -143$ dBm, and $P_p = -71$ dBm. As seen from this plot, the bandwidth of the parametric amplifier at fixed f_{0dc} is about 20 MHz. This value does not depend much on f_{0dc} , and is comparable to the linewidth of the cavity.

The noise temperature T_N is another important figure of merit. In Fig. 3a, the pump increases the signal level by 14 dB, but hardly changes the background noise level, which is limited by T_N^{HEMT} . This implies that $T_N^{\text{HEMT}} > (T_{Ni} + T_N)G_{nd}/L$, where T_{Ni} is the input noise temperature, G_{nd} is the gain of the parametric amplifier operated in the nondegenerate mode, and L is the small loss in the chain of the components between the output of the parametric amplifier and the input of the HEMT amplifier. Here, T_{Ni} should be almost equal to that of the vacuum noise $hf_s/2k_B = 0.26$ K, and $G_{nd} \geq 10^{1.4-0.3}$, where the factor $10^{-0.3}$ is due to the fact that the gain in the degenerate mode can be 3 dB larger than in the nondegenerate mode.¹⁷ We estimate L to be less than $10^{0.2}$. Consequently, the upper bound of T_N is estimated to be

0.87 K. We are planning more precise measurements using calibrated noise sources.

In summary, we have designed and operated a flux-driven Josephson parametric amplifier. The band center of the amplifier is demonstrated to be widely tunable. We operated it at different band centers and observed amplification and deamplification depending on the rel-

ative phase between the pump and the signal. The noise temperature is estimated to be less than 0.87 K.

The authors would like to thank Y. Yamamoto for fruitful discussions. They also would like to thank O. Astafiev, V. Bolkhovskiy, and E. Macedo for technical assistance.

-
- ¹ H. Takahashi, in *Advances in Communication Systems*, edited by A. V. Balakrishnan (Academic, New York, 1965), p. 227.
 - ² C. M. Caves, Phys. Rev. D **26**, 1817 (1982).
 - ³ A. Barone and G. Paterno, *Physics and applications of the Josephson effect* (Wiley, New York, 1982), chap. 11.
 - ⁴ R. Movshovich, B. Yurke, P. G. Kaminsky, A. D. Smith, A. H. Silver, R. W. Simon, and M. V. Schneider, Phys. Rev. Lett. **65**, 1419 (1990).
 - ⁵ B. Abdo, E. Segev, O. Shtempluck, and E. Buks, Appl. Phys. Lett. **88**, 022508 (2006).
 - ⁶ E. A. Tholén, A. Ergül, E. M. Doherty, F. M. Weber, F. Grégis, and D. B. Haviland, Appl. Phys. Lett. **90**, 253509 (2007).
 - ⁷ M. A. Castellanos-Beltrán and K. W. Lehnert, Appl. Phys. Lett. **91**, 083509 (2007).
 - ⁸ Y. Nakamura, Y. A. Pashkin, and J. S. Tsai, Nature **398**, 786 (1999).
 - ⁹ A. Wallraff, D. I. Schuster, A. Blais, L. Frunzio, R.-S. Huang, J. Majer, S. Kumar, S. M. Girvin, and R. J. Schoelkopf, Nature **431**, 162 (2004).
 - ¹⁰ T. Ojanen and J. Salo, Phys. Rev. B **75**, 184508 (2007).
 - ¹¹ In the current-pumping scheme, the pump modulates Josephson inductance only quadratically unless the SQUID is biased by a dc current. Therefore, in the degenerate-mode operation, the frequencies of the pump and the signal are equal.⁷
 - ¹² M. Wallquist, V. S. Shumeiko, and G. Wendin, Phys. Rev. B **74**, 224506 (2006).
 - ¹³ M. Sandberg, C. M. Wilson, F. Persson, T. Bauch, G. Johansson, V. Shumeiko, T. Duty, and P. Delsing, Appl. Phys. Lett. **92**, 203501 (2008).
 - ¹⁴ The quality factor is flux dependent. It tends to be smaller as we approach $\Phi/\Phi_0 = 0.5$. For example, it is 170 for $\Phi/\Phi_0 = 0.42$.
 - ¹⁵ The maximum gain increases as we increase P_p . However, the device becomes unstable if we increase P_p too much, which prevented us from making the maximum gain much higher than 14 dB.
 - ¹⁶ B. Yurke, P. G. Kaminsky, R. E. Miller, E. A. Whittaker, A. D. Smith, A. H. Silver, and R. W. Simon, Phys. Rev. Lett. **60**, 764 (1988).
 - ¹⁷ B. Yurke and E. Buks, J. Lightwave Tech. **24**, 5054 (2006).